

Figure S1. UV-visible light absorption spectral properties of coronaviral spike antigen constructs. (A) *Left:* Analysis of recombinant coronaviral spike and S1 constructs used in this work by SDS PAGE. Each lane contained 5 μg of purified recombinant protein; the gel was stained with Coomassie Blue. *Middle:* A representative SARS-CoV-2 S1 sample at ~ 4 mg/ml in a centrifugal concentrator. *Right:* Light absorbance spectra of four independent SARS-CoV-2 S1 batches (250-800 nm). (B-E) Spectra of stabilised trimeric SARS-CoV-2 spike ectodomain (residues 1-1208), NTD (1-310), RBD (319-541), and biliverdin (B); SARS-CoV-1 S1 (residues 1-518), HCoV NL63 S1 (residues 1-664) and OC43 S1 (1-665) (C); SARS-CoV-2 S1 purified under acidic conditions in sodium acetate pH 5.2 or dialysed overnight against suspension of activated charcoal. Note the retention of biliverdin in dialysed sample, consistent with high affinity of the interaction at pH 8.0 (D); H207A, R190K and N121Q SARS-CoV-2 S1 (E), compared to a representative spectrum of WT SARS-CoV-2 S1 purified under standard conditions, shows as black lines. Spectra were acquired from proteins diluted to 1-1.2 mg/ml in HBSE buffer and normalised to absorption at 278 nm.

Figure S2. Identification biliverdin IX α by mass spectrometry. Positive-mode ion chromatograms of biliverdin XI α standard and of the pigment isolated from recombinant S1 (*top left*) and structure proposal for some of the fragment ions of biliverdin XI α (*top*

right). The bottom panels show comparison of positive and negative MS2 spectra of the ions corresponding to biliverdin IX α in a standard (*upper*) and in recombinant S1 (*lower*). Black diamonds indicate expected positions of intact ions.

Figure S3. Representative SPR sensorgrams (A-I), estimates of equilibrium binding affinities (J) and melting point analysis (K). The sensorgrams were recorded with WT (A-E), R190K (F), or N121Q (G-H) SARS-CoV-2 S1, or WT SARS-CoV-1 S1 (I). The proteins were immobilised on a sensor chip and binding and dissociation of biliverdin IX α (A, E-G, I), bilirubin (B, H), hemin (C), and protoporphyrin IX (D) was measured. The analytes were injected at indicated concentrations at pH 8.0 (A-D, F-I) or pH 5.0 (E). The plots in panel H show representative normalised equilibrium binding curves; continuous black lines indicate fitting curves. Estimated K_{as} values are given in Table S1. Panel K shows melting behaviour of isolated SARS-CoV-2 NTD diluted to 30 μ M in HBSE buffer (150 mM NaCl, 1 mM EDTA, 20 mM HEPES-NaOH, pH8.0) in the absence or presence of 100-1,000 μ M biliverdin. The vertical axis corresponds to the first derivative of the ratios of fluorescence intensities measured at 350 and 330 nm wavelengths; the resulting melting points along with standard deviations ($n = 4$) are given in the inset.

Figure S4. Cryo-EM image processing for the SARS-CoV-2 spike-biliverdin complex. (A) Representative 2D classes corresponding to trimeric (*left*) and dissociated (*right*) spike single particles. (B) Trimeric spikes identified by 2D classification (371,422 particles) were subjected to 3D classification in Relion-3.1 into 11 classes. Particles belonging to 3RBDs-down and 1RBD-up forms of the spike (indicated with red and blue boxes, respectively) were combined and used for 3D reconstruction in CryoSPARC-2. (C) Fourier shell

correlations for the final reconstructions from CryoSPARC-2. **(D)** Maps colored by local resolution, as shown on the inset.

Figure S5. Stereo views of the cryo-EM and crystal structure density maps. Panel **A** shows the cryo-EM map of the 3RBD-down spike with biliverdin (*top*) and *2Fo-Fc* map of NTD-biliverdin complex crystal structure (*bottom*). The crystal structure is shown as sticks, coloured as in Fig. 1. Selected amino acid residues are indicated on the black-and-white image (*bottom right*). Electron density is contoured at r.m.s.d. of 1.0. Panel **B** shows cryo-EM map of the spike-Fab complex. Protein chains are depicted as ribbons, colored as in Fig. 4. Selected side chains are shown as sticks. Positions of selected residues, the gate and the lip are indicated on the back-and-white images to the right.

Figure S6. Evidence of biliverdin presence in previous SARS-CoV-2 spike cryo-EM reconstructions. Four published structures (*14-17*) with map features associated with the NTD and not explained by the original models are shown as chicken wire. In each case, a biliverdin molecule was placed by superposition of the NTD-biliverdin complex crystal structure.

Figure S7. Infectivity of lentiviral vectors pseudotyped with SARS-CoV-2 spike with and without indicated mutations within the NTD on Vero (*left*) and Huh7 (*right*) cells. Infectivity is expressed as number of infected cells relative to the amount of RT-activity associated to the virus inoculum. Bars represent means and data from individual measurements ($n = 4$) are shown with dots. Error bars represent standard deviation of the mean calculated from the quadruplicate determinations.

Figure S8. (A) Gating strategy of HEK293T cells transfected to express WT spike or N121Q SARS-CoV-2 spike. Staining intensity was taken as the MFI of positively stained cells, represented by the rectangular gates. (B-C) MFI of IgM (B) and IgA (C) staining of HEK293T cells expressing WT or N121Q SARS-CoV-2 spike by individual patient sera in the absence or the presence of 10 μ M biliverdin. Each symbol represents an individual patient (n=17) and coloured dotted lines represent the linear regression for each spike variant. (D-E) Change in MFI caused by the addition of 10 μ M biliverdin, as percent of staining without biliverdin, for serum for IgM and IgA antibodies. Each pair of connected symbols represents an individual patient.

Figure S9. Effect of biliverdin binding on reactivity of SARS-CoV-2 with convalescent sera. IgG capture ELISA was performed with recombinant WT (biliverdin-depleted, red circles) or N121Q (blue circles) S1 antigen using sera from SARS-CoV-2 infected and convalescent individuals (n=91) in the presence (vertical axis) or absence (horizontal axis) of 10 μ M biliverdin. Dotted lines represent linear fit for each set (considering samples with OD values <2.5, n = 82); the grey line is the diagonal. The inset shows posterior probability density plots of values for pairwise contrasts (\pm biliverdin) for the WT and N121Q S1 proteins. Black dots indicate the median of the distribution, thick and thin line ranges correspond to the 85% and 95% highest density interval, respectively; the dotted vertical line indicates a zero difference. Antibodies binding to S1 epitopes, which are occluded within protein-protein interfaces of the full-length trimeric spike, contribute to the observed signal in this ELISA assay. Therefore, the signal differences (\pm biliverdin) are expected to be less pronounced than in the flow cytometry assay, which used the complete native spike (Fig. 2).

Figure S10. Biliverdin decreases binding to SARS CoV-2 spike by a group of human monoclonal IgGs. (A) Antibodies observed previously to bind to spike were titrated 6-fold and assayed by IgG ELISA for binding to WT S1 or N121Q S1. WT protein was prepared under acidic conditions to remove any co-purifying biliverdin, and was used in the absence (-biliverdin) or presence (+biliverdin) of 10 μ M exogenous biliverdin. Area under the curve (AUC) is shown for 38 IgG that bound to S1 (also see Figs 3A and 3C). AUC values are colour-coded as per the key. Fold change compared to WT S1 protein are reported. (B) IC₅₀ values in μ g/ml calculated in Graphpad Prism are shown for each combination of IgG and viral preparation. The fold change column shows the decrease in IC₅₀ with BLV relative to either wild-type S pseudotyped or live virus. Colour-coding is indicated in the key.

Figure S11. Cryo-EM image processing for the spike-Fab complex. (A) Representative 2D classes corresponding to trimeric (*left*) and dissociated (*right*) spike single particles. (B) Trimeric spikes identified by 2D classification (709,127 particles) were subjected to 3D classification in Relion-3.1 into 16 classes. Particles belonging to a class corresponding to trimeric spike (1RBD-up) with single Fab bound (boxed) were used in final 3D reconstruction in CryoSPARC-2. (C) Fourier shell correlations for the final reconstructions from CryoSPARC-2. (D) Cryo-EM map colored by local resolution.

Movie S1. Conformational changes in the NTD associated with binding neutralising antibody P008_056.

Figure 1

medRxiv preprint doi: <https://doi.org/10.1101/2021.01.21.21249203>; this version posted January 26, 2021. The copyright holder for this preprint (which was not certified by peer review) is the author/funder, who has granted medRxiv a license to display the preprint in perpetuity. It is made available under a [CC-BY-NC-ND 4.0 International license](https://creativecommons.org/licenses/by-nc-nd/4.0/).

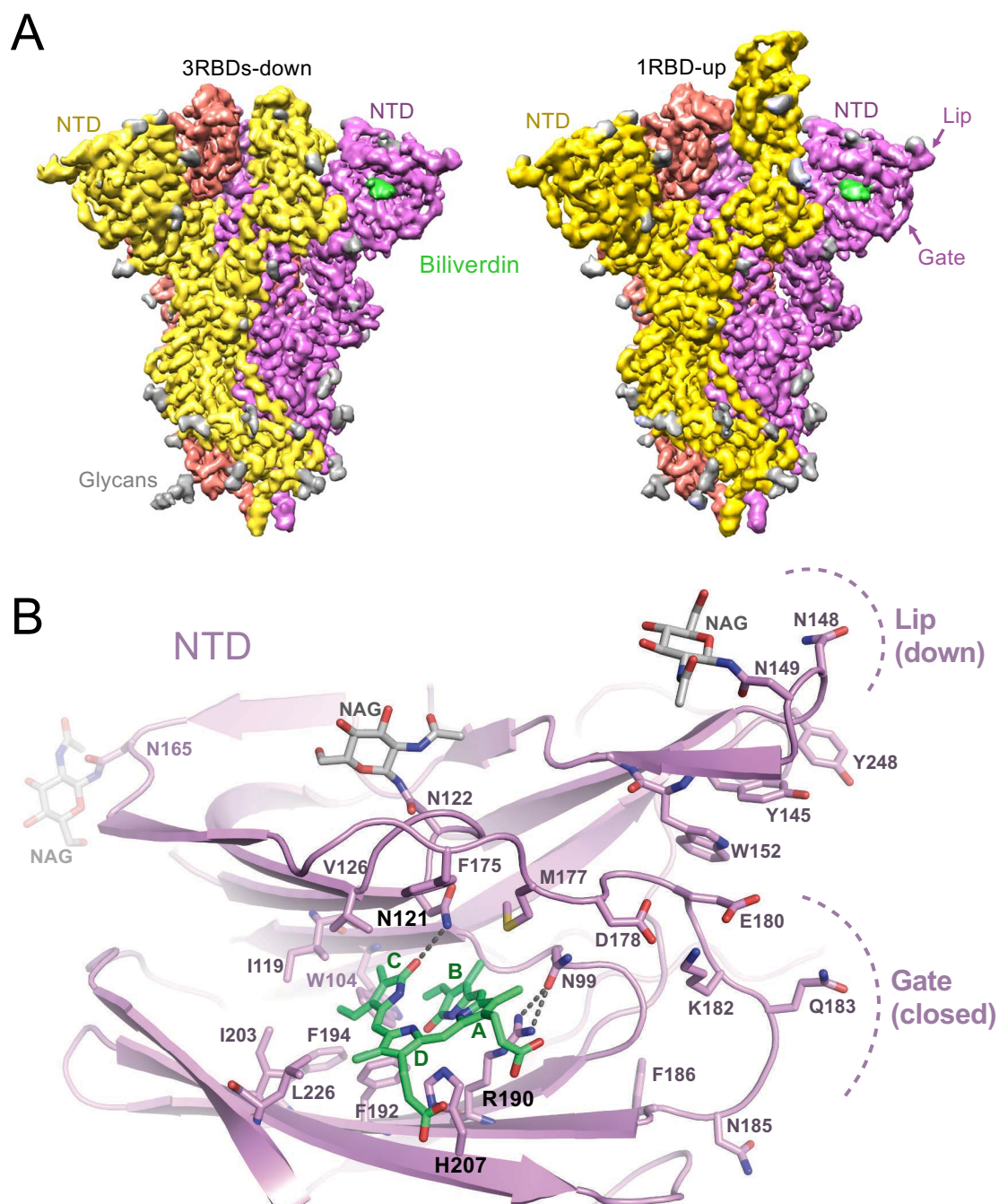


Figure 2

medRxiv preprint doi: <https://doi.org/10.1101/2021.01.21.21249203>; this version posted January 26, 2021. The copyright holder for this preprint (which was not certified by peer review) is the author/funder, who has granted medRxiv a license to display the preprint in perpetuity. It is made available under a [CC-BY-NC-ND 4.0 International license](https://creativecommons.org/licenses/by-nc-nd/4.0/).

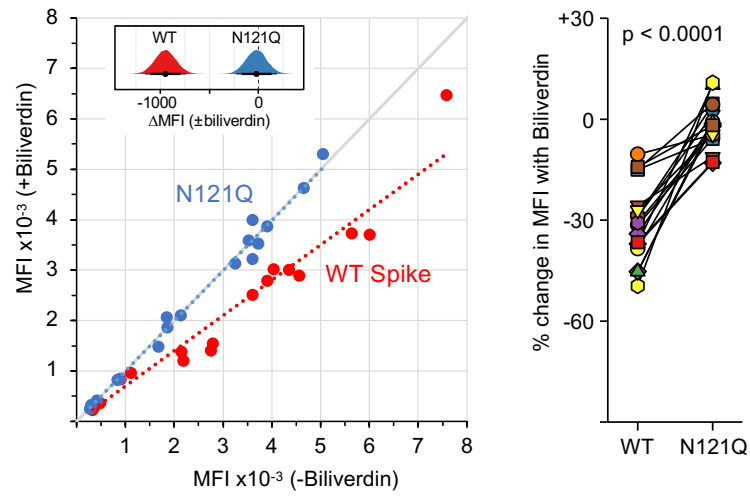


Figure 3

medRxiv preprint doi: <https://doi.org/10.1101/2021.01.21.21249203>; this version posted January 26, 2021. The copyright holder for this preprint (which was not certified by peer review) is the author/funder, who has granted medRxiv a license to display the preprint in perpetuity. It is made available under a [CC-BY-NC-ND 4.0 International license](https://creativecommons.org/licenses/by-nc-nd/4.0/).

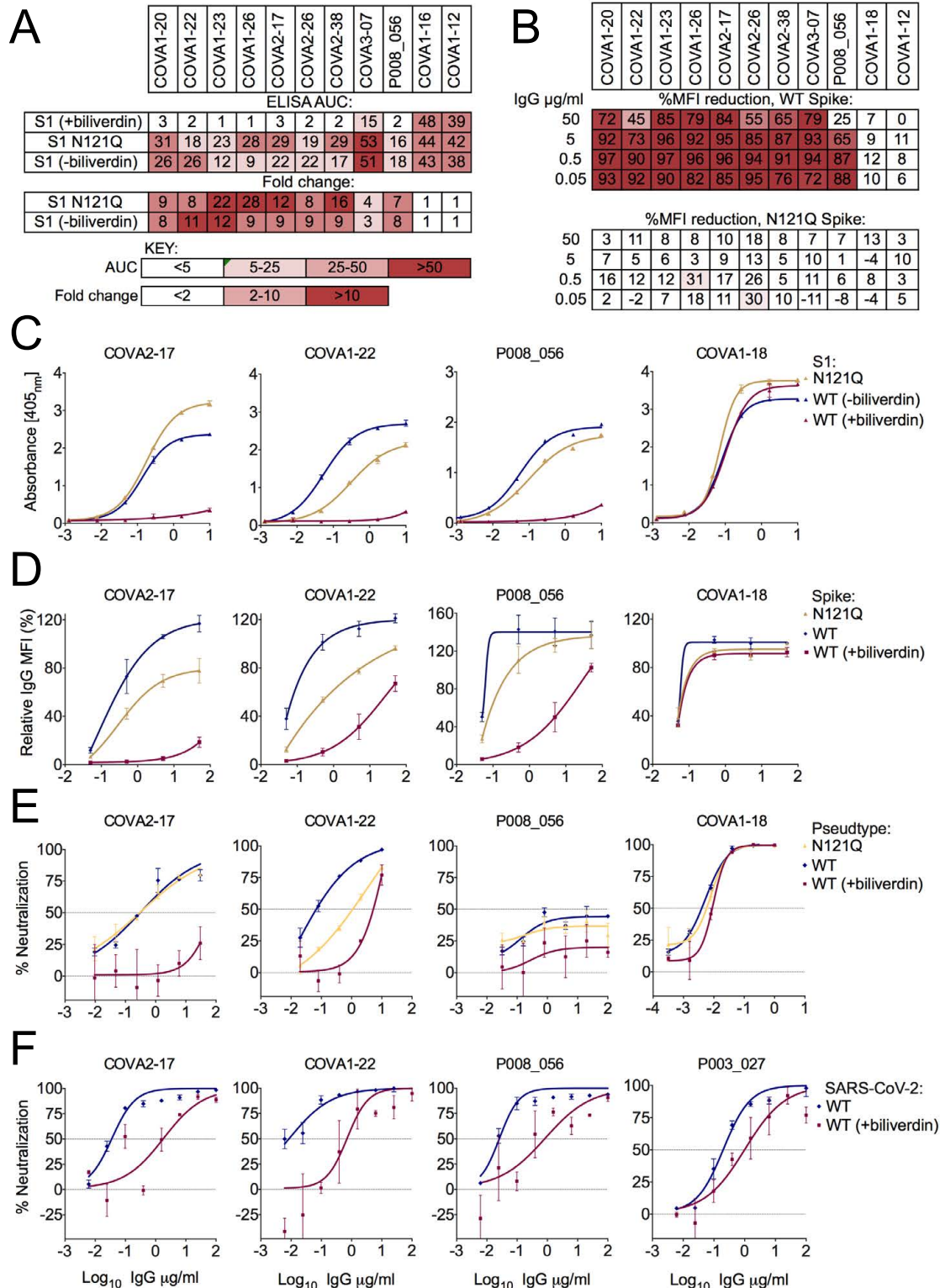
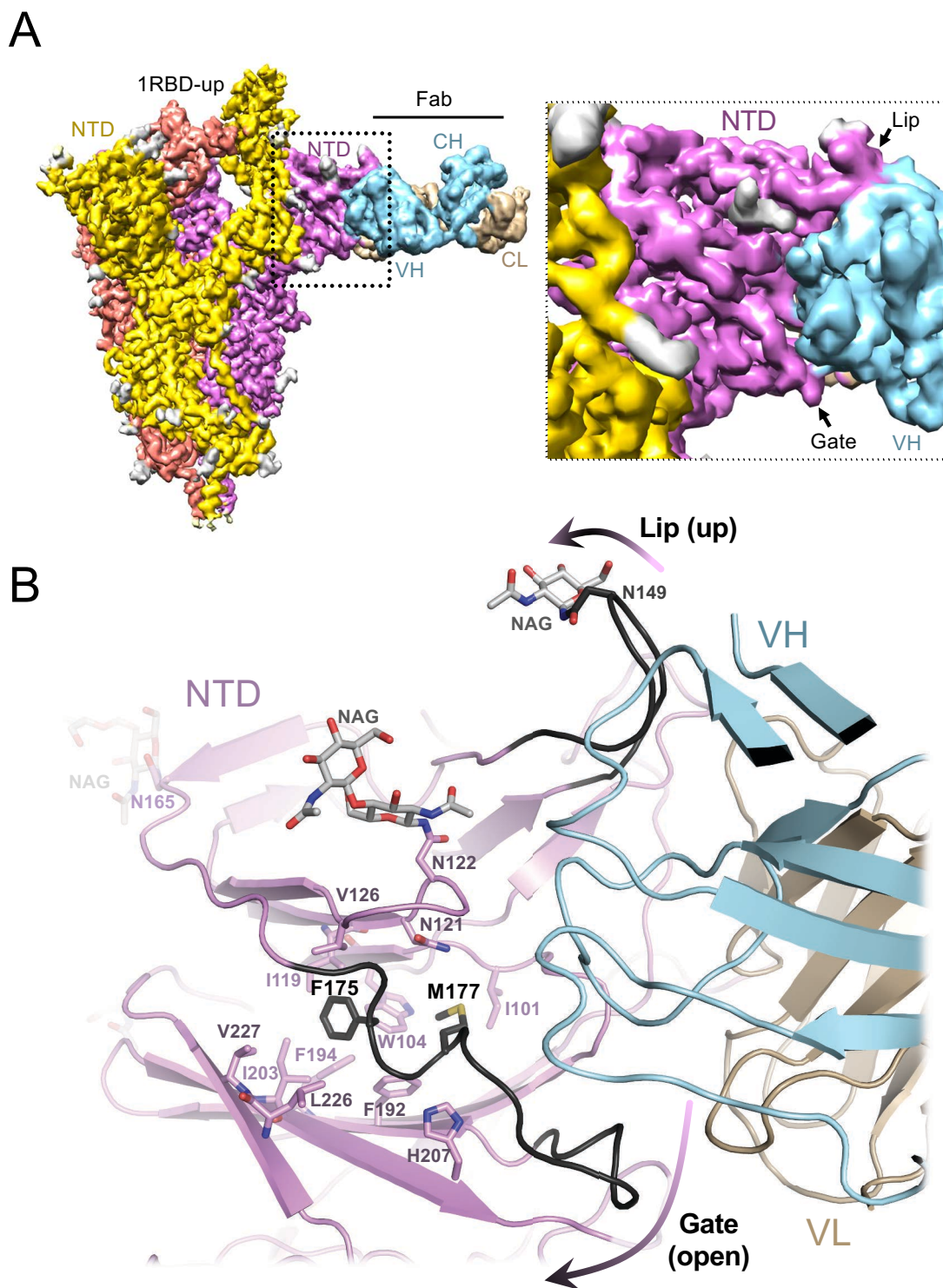


Figure 4

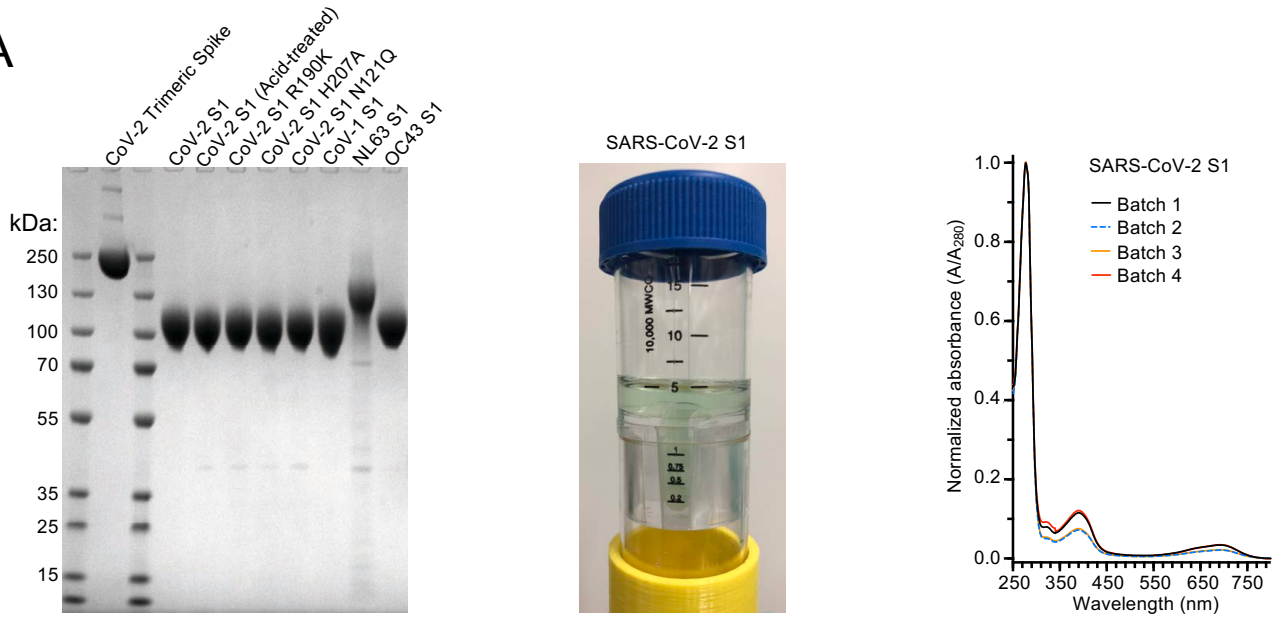
medRxiv preprint doi: <https://doi.org/10.1101/2021.01.21.21249203>; this version posted January 26, 2021. The copyright holder for this preprint (which was not certified by peer review) is the author/funder, who has granted medRxiv a license to display the preprint in perpetuity. It is made available under a [CC-BY-NC-ND 4.0 International license](https://creativecommons.org/licenses/by-nc-nd/4.0/).



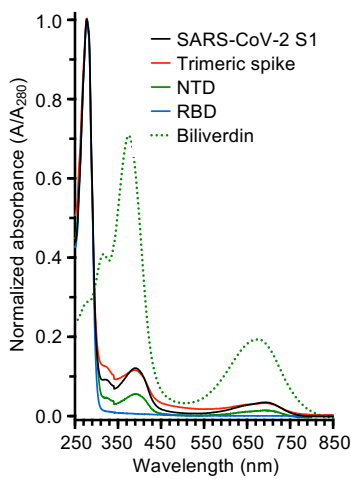
Supplementary Figure 1

medRxiv preprint doi: <https://doi.org/10.1101/2021.01.21.21249203>; this version posted January 26, 2021. The copyright holder for this preprint (which was not certified by peer review) is the author/funder, who has granted medRxiv a license to display the preprint in perpetuity. It is made available under a [CC-BY-NC-ND 4.0 International license](https://creativecommons.org/licenses/by-nc-nd/4.0/).

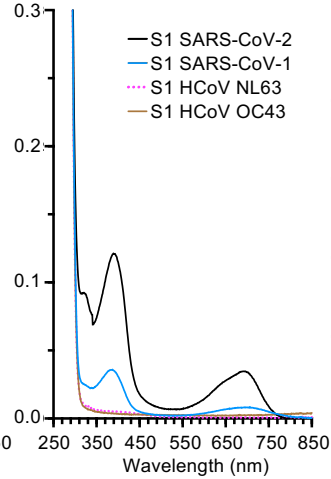
A



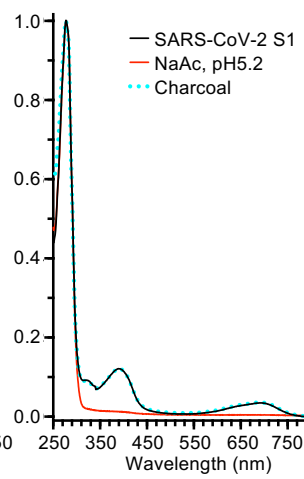
B



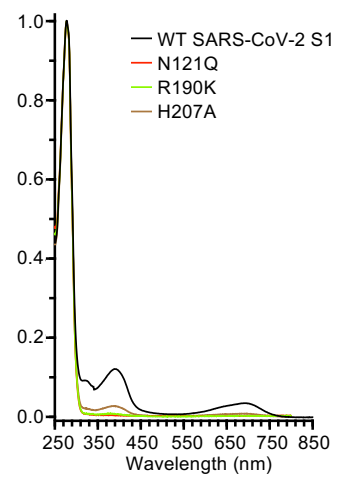
C



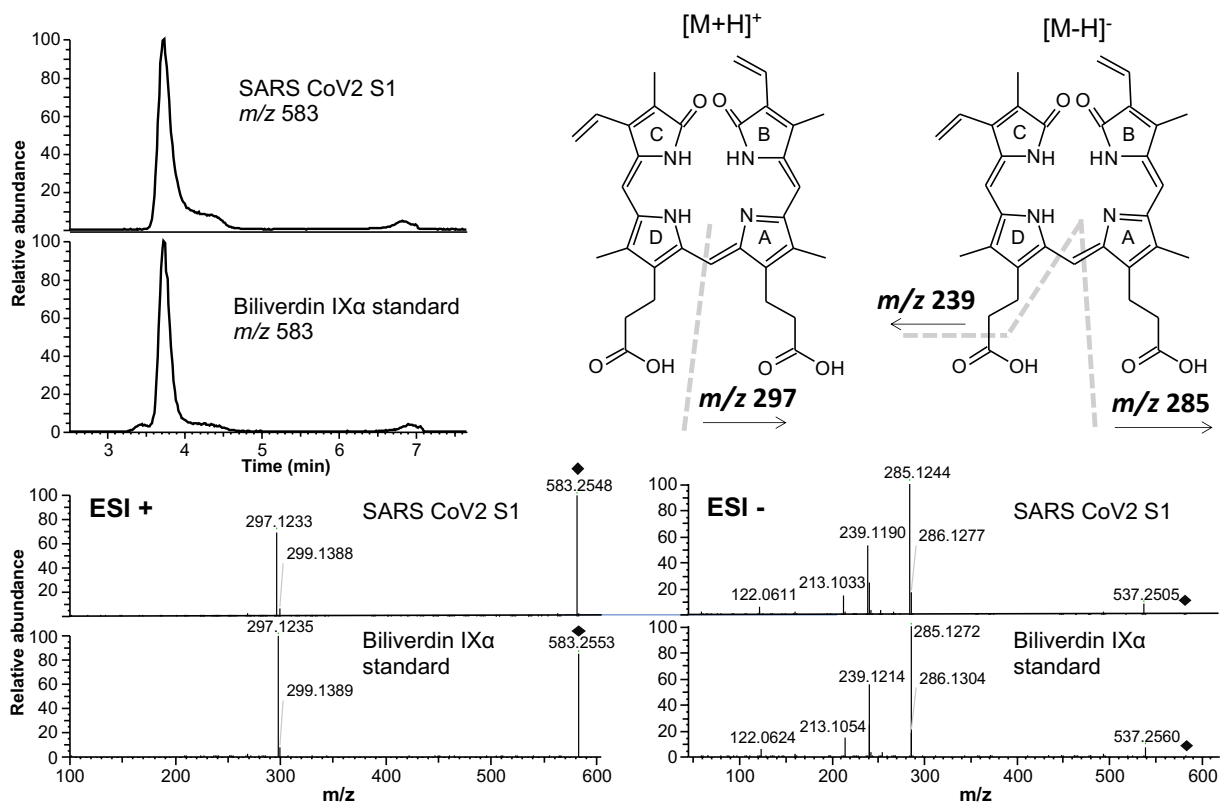
D



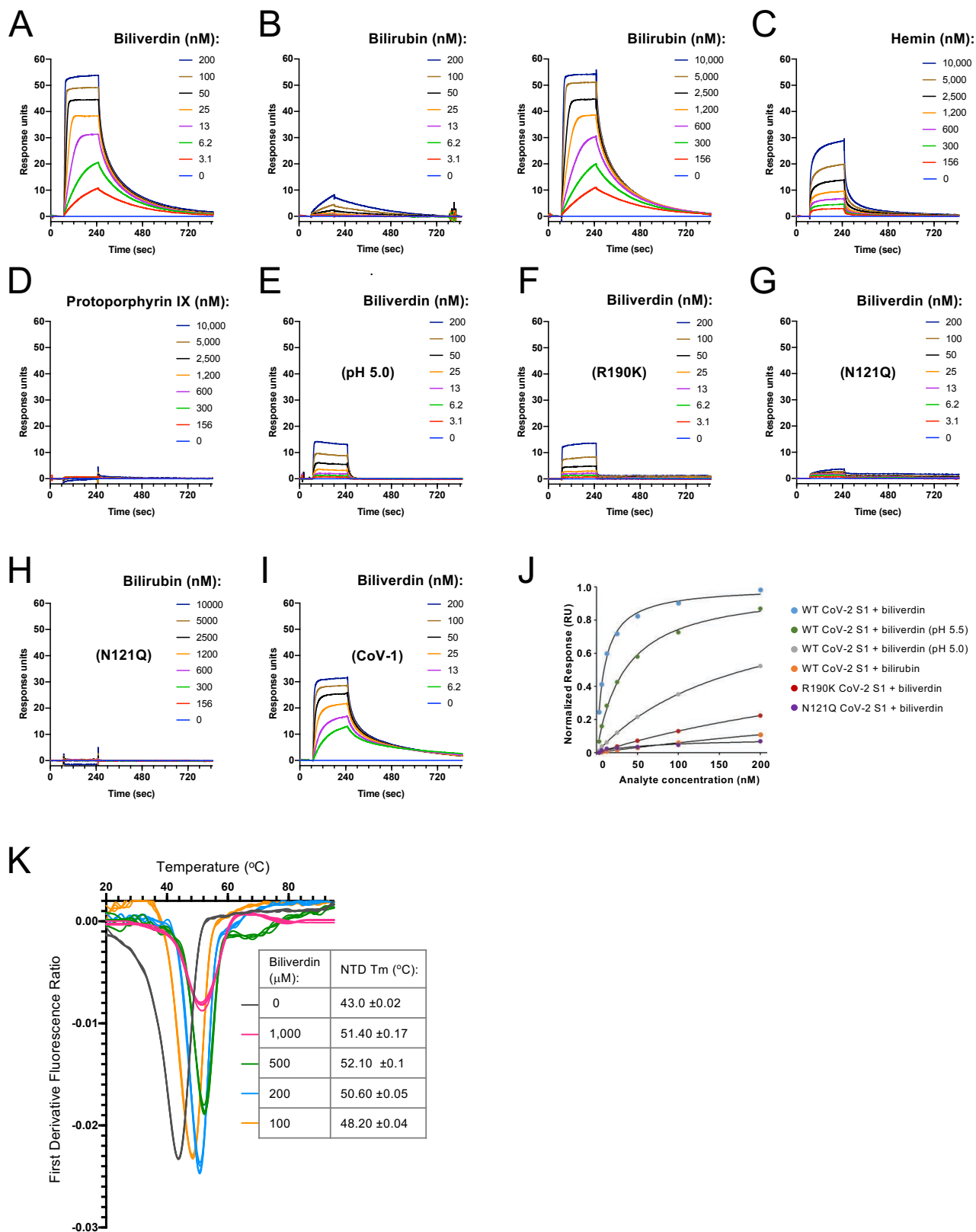
E



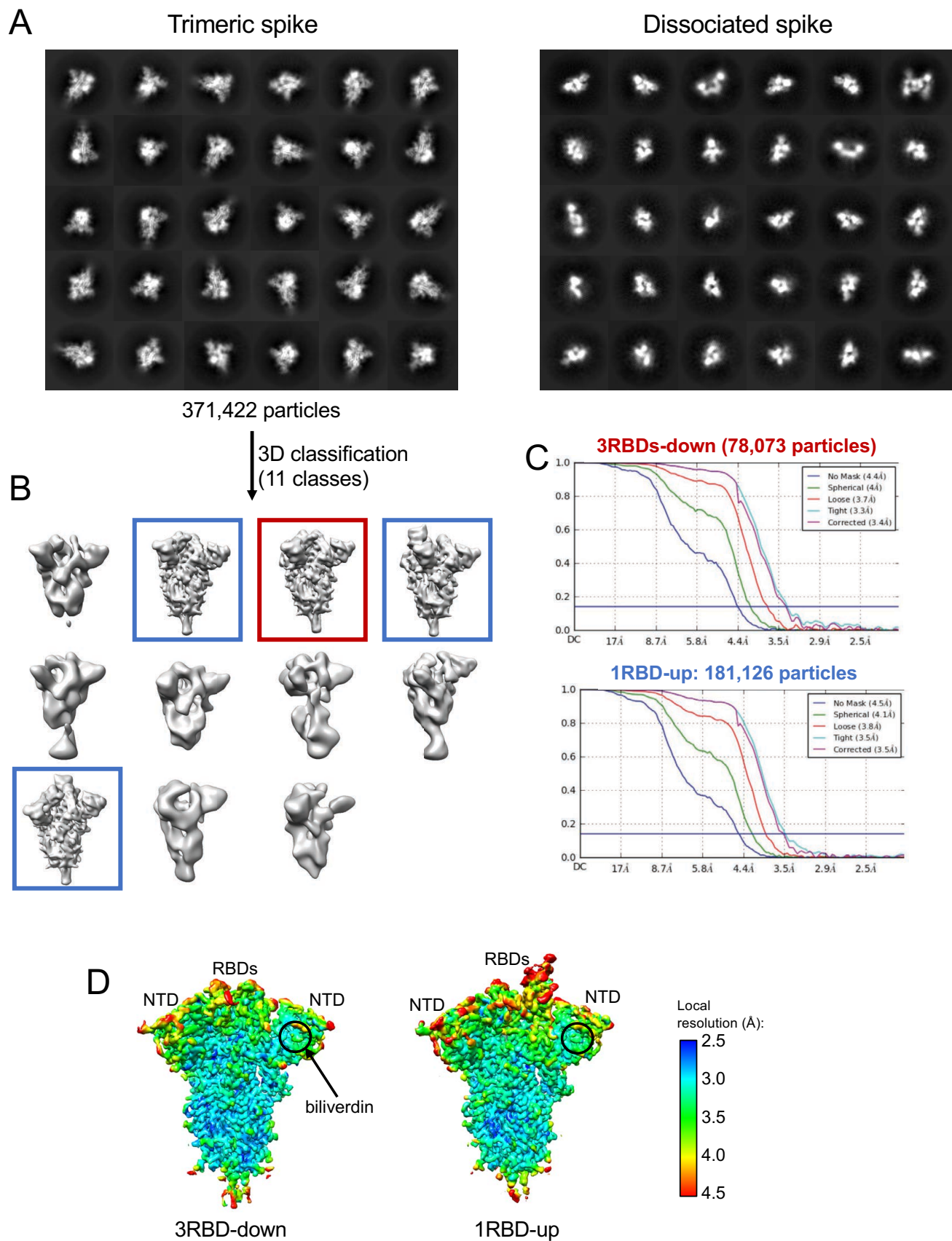
Supplementary Figure 2



Supplementary Figure 3

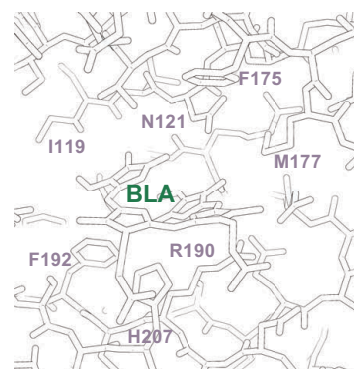
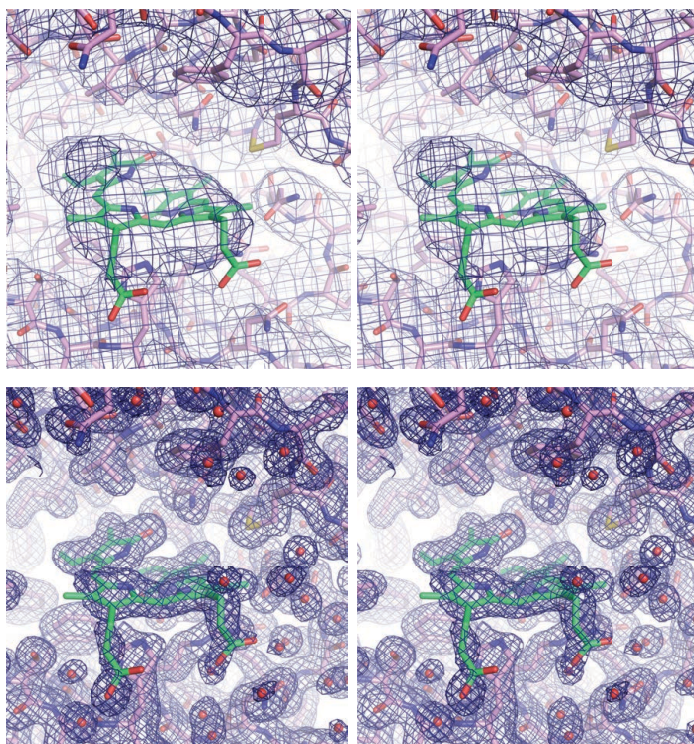


Supplementary Figure 4

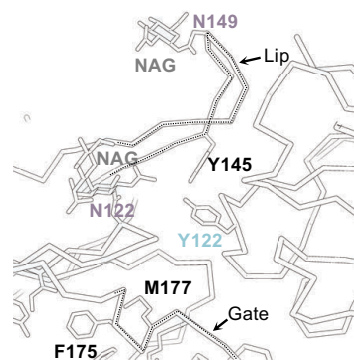
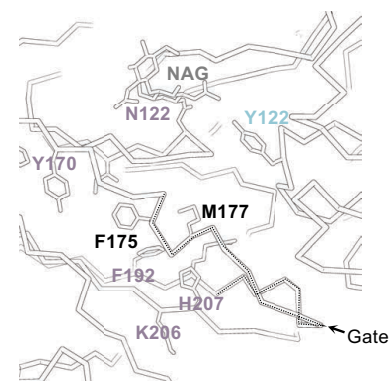
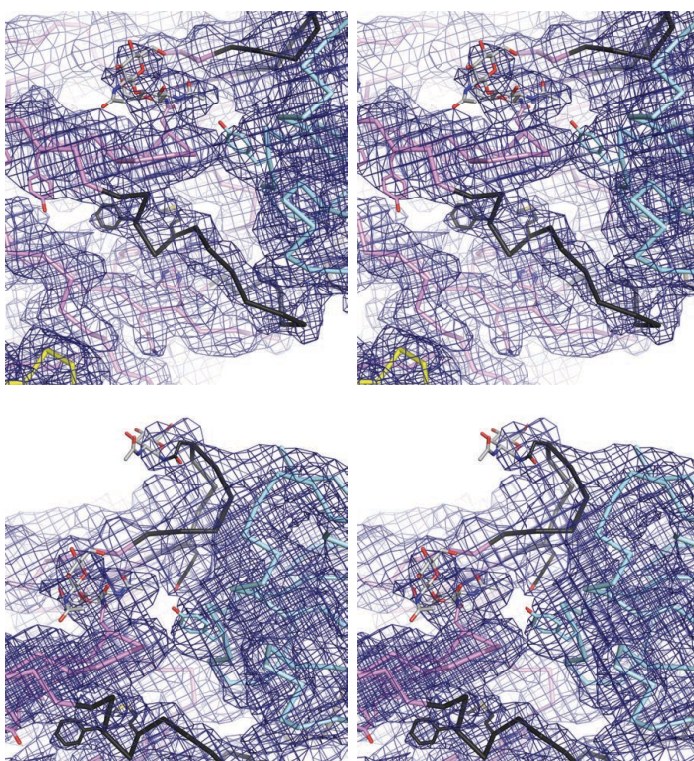


Supplementary Figure 5

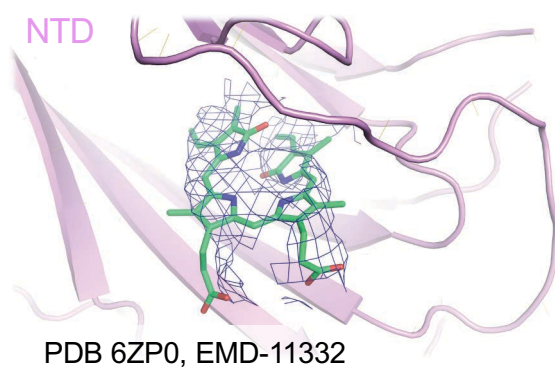
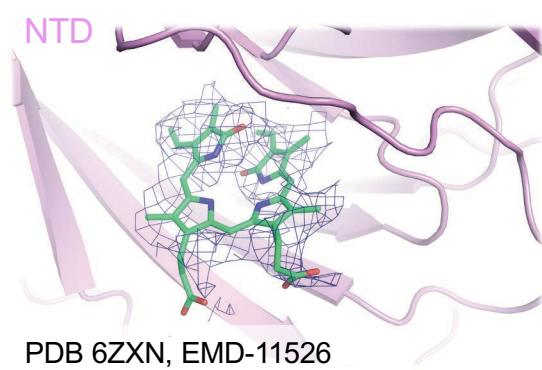
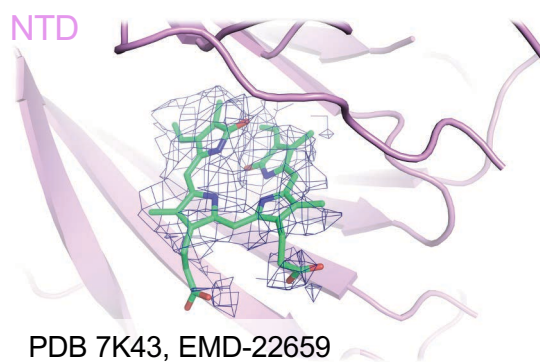
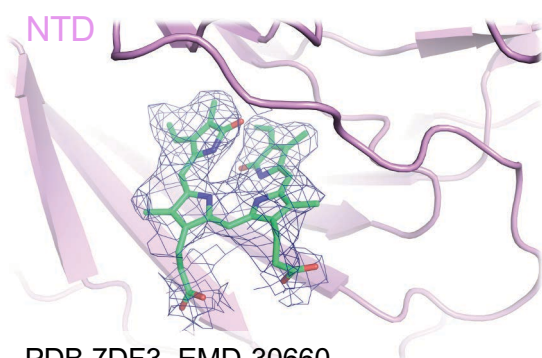
A



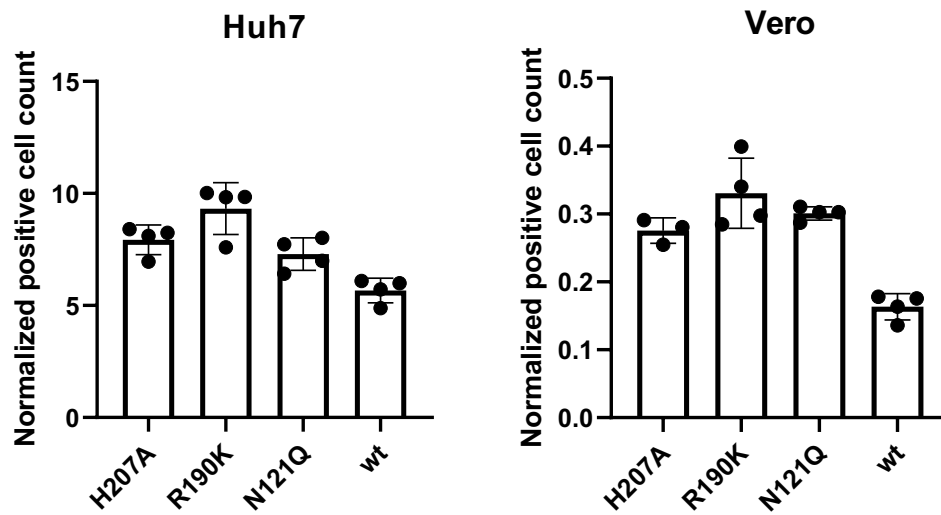
B



Supplementary Figure 6

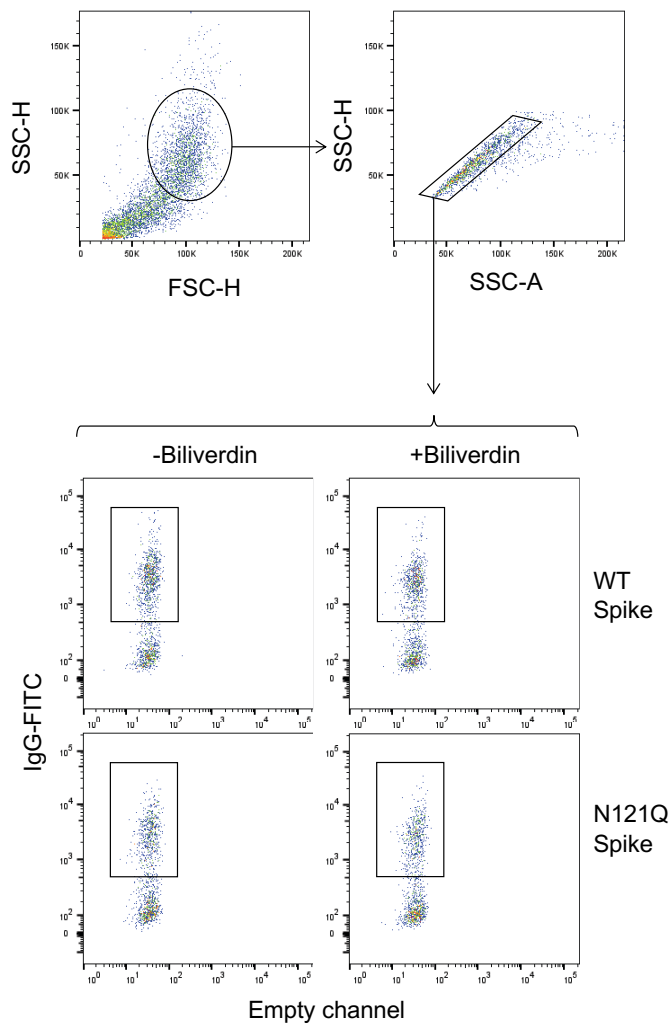


Supplementary Figure 7

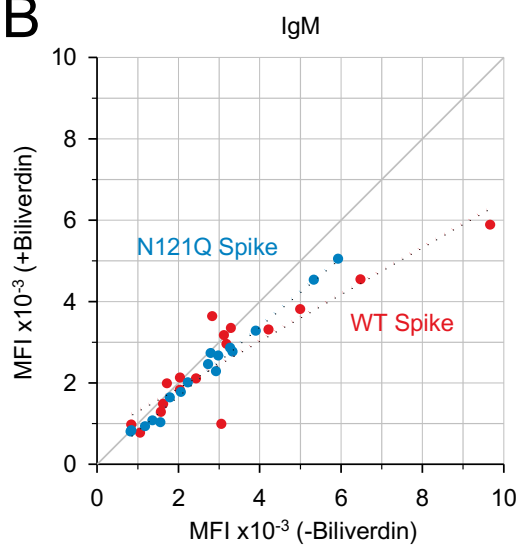


Supplementary Figure 8

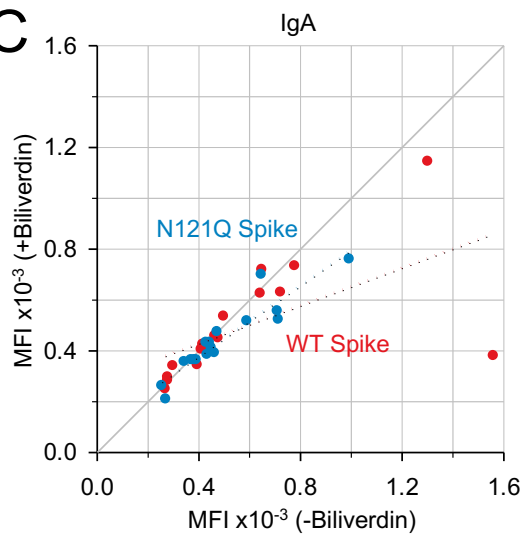
A



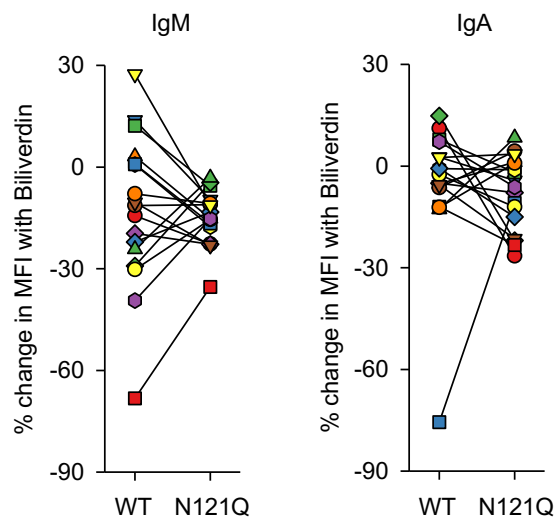
B



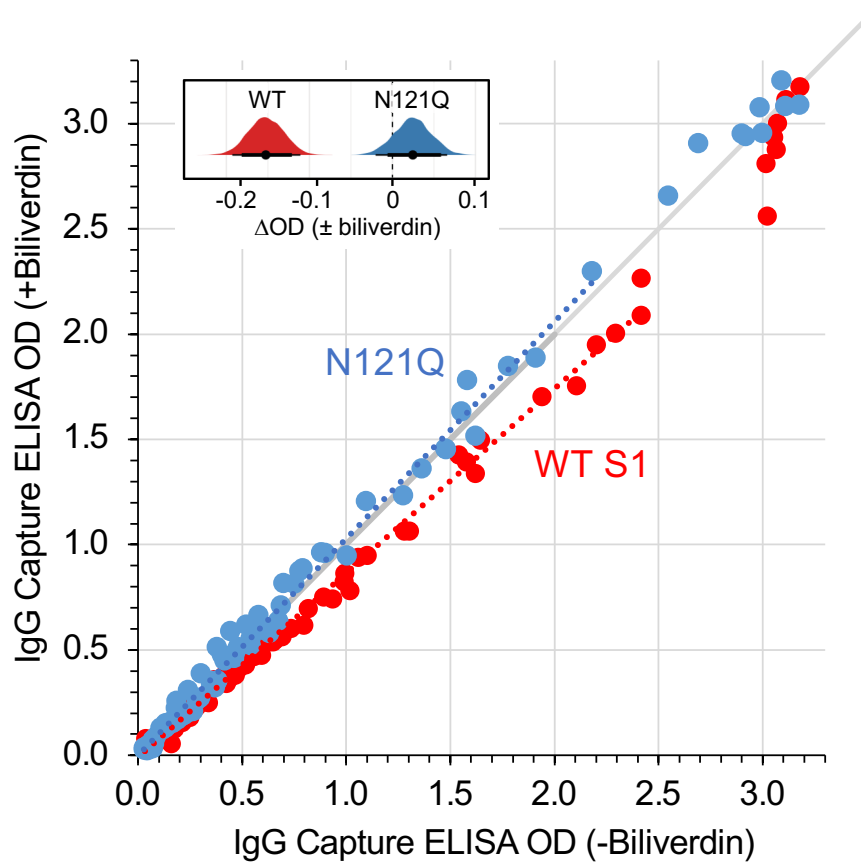
C



D



Supplementary Figure 9



Supplementary Figure 10

A

COVA1-20	COVA1-22	COVA1-23	COVA1-26	COVA2-03	COVA2-10	COVA2-25	COVA2-26	COVA2-30	COVA2-38	COVA3-07	P003_027	P003_055	P008_039	P008_051	P008_052	P008_056	COVA1-12	COVA1-16	COVA1-18	COVA2-01	COVA2-02	COVA2-04	COVA2-07	COVA2-11	COVA2-15	COVA2-17	COVA2-29	COVA2-39	COVA2-44	COVA2-46	P003_014	P008_017	P008_057	P008_081	P008_087	P008_100	P008_108
----------	----------	----------	----------	----------	----------	----------	----------	----------	----------	----------	----------	----------	----------	----------	----------	----------	----------	----------	----------	----------	----------	----------	----------	----------	----------	----------	----------	----------	----------	----------	----------	----------	----------	----------	----------	----------	----------

ELISA AUC:

WT (+biliverdin)	3	2	1	1	44	39	50	2	42	2	15	38	33	43	38	39	2	39	48	35	28	44	44	70	71	48	3	50	39	50	39	36	37	39	41	43	42	40
N121Q	31	18	23	28	61	73	46	19	33	29	53	37	32	44	39	39	16	42	44	37	34	47	47	69	63	49	29	51	73	51	45	39	40	43	40	45	43	40
WT (-biliverdin)	26	26	12	9	37	63	43	22	38	17	51	42	34	44	39	41	18	38	43	32	31	42	42	75	69	45	22	48	63	48	44	38	39	43	41	45	44	40

Fold change:

N121Q	9	8	22	28	1	2	1	8	1	16	4	1	1	1	1	1	7	1	1	1	1	1	1	1	1	1	12	1	2	1	1	1	1	1	1	1	1	1	1
WT (-biliverdin)	8	11	12	9	1	2	1	9	1	9	3	1	1	1	1	1	8	1	1	1	1	1	1	1	1	1	9	1	2	1	1	1	1	1	1	1	1	1	1

B

	Pseudotype			
	N121Q Spike	WT Spike (+biliverdin)	WT Spike	Fold change
COVA2-17	0.31	>30	0.32	>90
COVA1-22	3.47	>10	0.02	>600
P008_056	>100	>100	>100	n/a
COVA1-18	0.01	0.01	0.01	2

	SARS-CoV-2		
	+biliverdin	WT	Fold change
COVA2-17	1.82	0.04	51
COVA1-22	0.72	0.01	81
P008_056	0.85	0.03	33
P003_027	0.26	0.05	5

KEY

IC50	No activity	>1	0.1-1	<0.01
------	-------------	----	-------	-------

Fold change	0-5	5-50	50-500	>500
-------------	-----	------	--------	------

Supplementary Figure 11

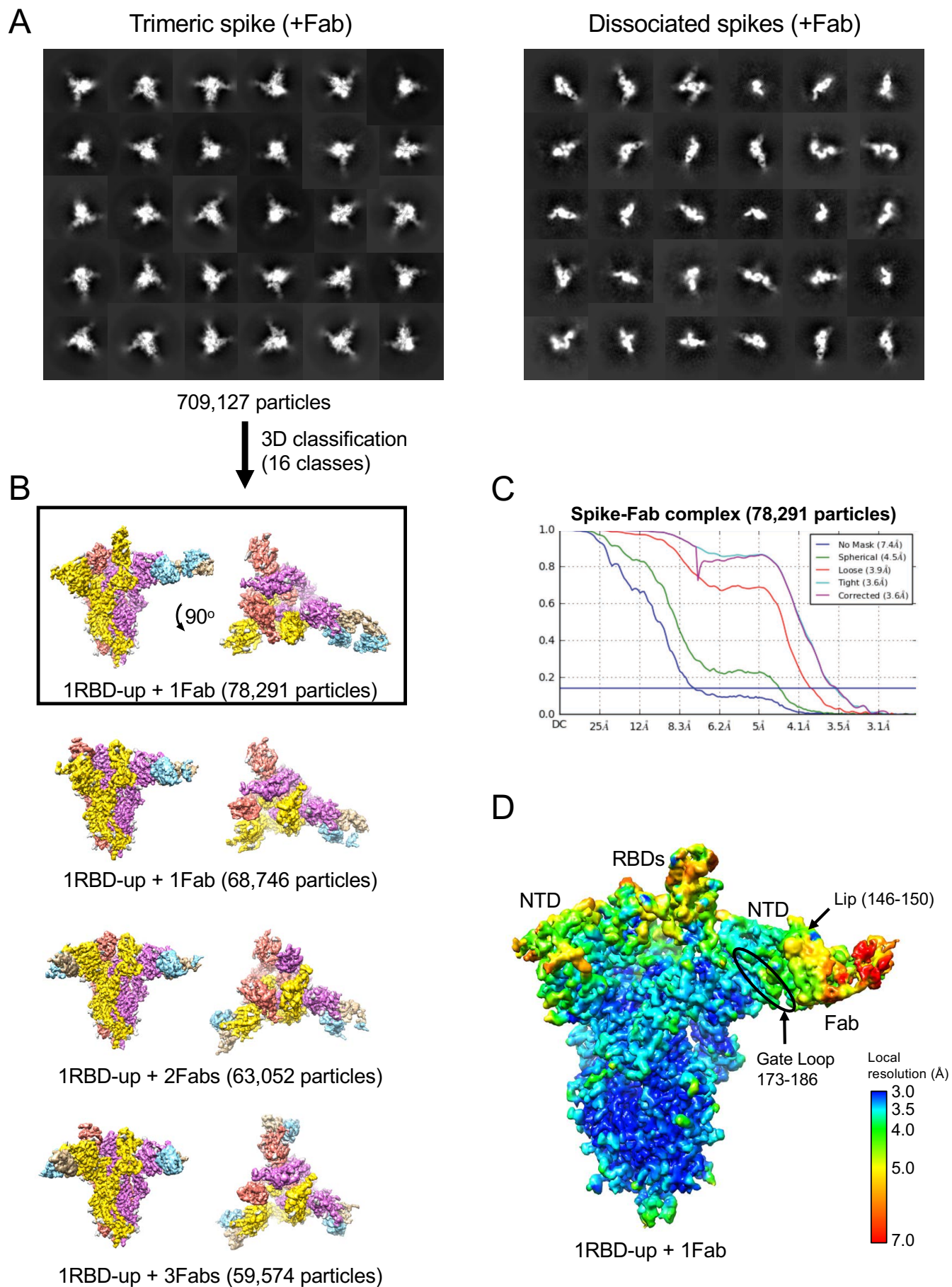


Table S1. Affinity of SARS CoV2 S1 interaction with tetrapyrroles measured using surface plasmon resonance.

S1 protein	Ligand	Buffer ¹	Kd (nM) ²	Mean Kd (nM) ³
WT, CoV-2	Biliverdin	Hepes pH 8.0	8.0; 9.2	9.8 ±1.3
WT, CoV-2	Biliverdin	1% DMSO, Hepes pH 8.0	10.6; 11.5	
WT, CoV-2	Biliverdin	1% DMSO, Hepes pH 7.0	13.5; 14.5	
WT, CoV-2	Biliverdin	1% DMSO, BTP pH 6.0	13.6; 14.2	
WT, CoV-2	Biliverdin	1% DMSO, BTP pH 5.5	34.5; 29.9	
WT, CoV-2	Biliverdin	1% DMSO, BT pH 5.0	186.8; 194.1; 358.5	250 ±100
WT, CoV-2	Bilirubin	1% DMSO, Hepes pH 8.0	540; 620;1,000	720 ±250
WT, CoV-2	Hemin	1% DMSO, Hepes pH 8.0	5,800; 6,640; 8,200	7,000 ±1,200
WT, CoV-2	Protoporphyrin	1% DMSO, Hepes pH 8.0	>10,000	`
WT, CoV-1	Biliverdin	Hepes pH 8.0	18.7; 19.6; 20.4	19.6 ±0.8
R190K, CoV-2	Biliverdin	Hepes pH 8.0	1,500; 2,230	
N121Q, CoV-2	Biliverdin	Hepes pH 8.0	16,800; 19,200	
N121Q, CoV-2	Bilirubin	1% DMSO, Hepes pH 8.0	>10,000	

¹Running buffer variables (DMSO and pH) are shown; full composition is given in Methods section. BTP, BisTris Propane; BT, BisTris.

²Results of individual experiments performed in equilibrium mode.

³Mean and standard deviation shown for $N > 2$ measurements.

Table S2. Cryo-EM data collection, refinement and validation statistics

	SARS CoV-2 Spike + biliverdin	SARS CoV-2 Spike + P008_056 Fab	
Data collection			
Magnification	128,440	36,232	
Voltage (keV)	300	300	
Electron exposure (e ⁻ /Å ²)	33.6	51	
Defocus range (µm)	-1.6 to -4	-1.6 to -4	
Pixel size (Å)	1.09	1.38	
3D reconstruction			
Molecular assembly	3RBDs-down	1RBD-up	1RBD-up + 1Fab
Initial particle images (no.)	1,209,334	1,209,334	2,505,265
Final particle images (no.)	78,073	181,126	78,291
Symmetry imposed	C3	C1	C1
Map resolution (Å)	3.36	3.5	3.6
FSC threshold	0.143	0.143	0.143
Map resolution range (Å)			
Refinement			
Model resolution (Å)	3.36	3.5	3.6
Model resolution range (Å)	2.5-4.5	2.5-6.0	3.0-7.0
Map sharpening <i>B</i> factor (Å ²)	-161	-156	-66
Model composition			
Nonhydrogen atoms	26,959	26,805	30,006
Protein residues	3,261	3,261	3,698
Ligands	BLA: 3; NAG: 84	BLA: 3, NAG:77	BLA: 2, NAG:79
<i>B</i> factors (Å ²)			
Protein	56.84	58.43	158.38
Ligand	94.84	91.87	147.91
R.m.s. deviations			
Bond lengths (Å)	0.003	0.003	0.004
Bond angles (°)	0.521	0.587	0.552
CC	0.794	0.793	0.82
Validation			
MolProbity score	1.59	1.66	1.84
Clashscore	6.08	6.86	7.28
Poor rotamers (%)	0.00	0.00	0.03
Ramachandran plot			
Favored (%)	96.23	95.8	93.11
Disallowed (%)	0	0	0.16

Table S3. X-ray data collection and refinement statistics.

	NTD with biliverdin
Data collection:	
Wavelength (Å)	1.00
Space group	C222 ₁
Unit cell parameters	
<i>a, b, c</i> (Å)	98.07, 100.19, 85.97
α, β, γ (°)	90, 90, 90
Number of crystals used	1
Resolution (Å)	50.10-1.82 (1.87-1.82) ^a
Number of reflections	
measured	510,757 (34,535)
unique	38,068 (2,758)
Completeness (%)	99.4 (98.6)
Multiplicity	13.4 (12.5)
$\langle I/\sigma(I) \rangle$	12.4 (1.1)
R_{merge} (%)	0.166 (2.407)
R_{pim} (%)	0.048 (0.721)
CC 1/2	0.999 (0.408)
Refinement statistics:	
Resolution range (Å)	49.03-1.82 (1.885-1.82)
Number of reflections	
total	38,038 (3,741)
free	1,917 (165)
$R_{\text{work}}/R_{\text{free}}$	0.1636/0.1997
Number of atoms	
total	3,096
protein	2,511
ligands	234
solvent	351
R.m.s. deviations from ideal	
bond lengths (Å)	0.01
bond angles (°)	1.0
Average B-factor (Å²)	32.76
Clash Score^b	5.32
Favored Rotamers^b	95.1
Ramachandran plot (%)^b	
favored	96.05
disallowed	0.00

^a Values in parentheses correspond to the highest resolution bin.

^b Analyzed using MolProbity (<http://molprobity.biochem.duke.edu/>).